INT. J. REMOTE SENSING, 1999, VOL. 20, no. 5, 1031–1038

Multi-temporal active-fire based burn scar detection algorithm

D. P. ROY

Department of Geography, University of Maryland, NASA Goddard Space Flight Center, Code 922, Greenbelt, MD 20771, USA

L. GIGLIO, J. D. KENDALL

Science Systems and Applications Inc., NASA Goddard Space Flight Center, Code 923, Greenbelt, MD 20771, USA

and C. O. JUSTICE

Department of Environmental Sciences, University of Virginia, Charlottesville, VA 22903, USA

(*Received 3 April 1998; in final form 19 October 1998*)

Abstract. A multi-temporal burn scar detection algorithm designed for global application is described and demonstrated using 24-daily AVHRR images of an area of savanna burning near the Okavango Delta, Southern Africa. The algorithm is computationally simple, does not use fixed thresholds except to detect saturated AVHRR pixels, and incorporates a recent active-fire detection algorithm. The algorithm provides the basis for operational burn scar monitoring using the AVHRR and MODIS.

1. Introduction

The area burned by fire is an important variable for estimating trace gas and particulate emissions required for global change research (Scholes *et al.* 1996). Until the launch of EOS sensors, such as the MODerate resolution Imaging Spectroradiometer (MODIS), the Advanced Very High Resolution Radiometer (AVHRR) provides the major source of data of appropriate spatial and temporal resolution to support global studies of biomass burning (Justice *et al.* 1993). Although a global fire data set derived from AVHRR 1 km data now exists (IGBP 1997) it cannot be used to infer reliably the area burned because burning may not occur at the time of satellite overpass.

Burned areas are characterized by deposits of charcoal and ash, by the removal of vegetation, and by the alteration of the vegetation structure. These changes are amenable to remote sensing but vary temporally and spatially because the type of vegetation that burns, the completeness of the burn, the post fire evolution and revegetation of the burned area and the rate of charcoal and ash dissipation by the elements vary as a function of several biophysical and anthropogenic factors. The utility of wide field of view, polar orbiting sensors (e.g. AVHRR, MODIS) for burned area mapping is reduced by changes in the effective spatial resolution as a function

International Journal of Remote Sensing
ISSN 0143-1161 print/ISSN 1366-5901 online
http://www.tandf.co.uk/JNLS/res.htm
http://www.taylorandfrancis.com/JNLS/res.htm

of the sensing geometry (Wolfe *et al.* 1998), by variations in the sensor response between consecutive orbits and across the image swath due to surface anisotropy (Meyer *et al.* 1995), and by cloud, atmospheric, and smoke contamination (Pereira 1999).

A comprehensive review of burn scar detection techniques is found in Pereira *et al.* (1997). With the exception of Barbosa *et al.* (1997) the authors are unaware of an automated burned area mapping algorithm applicable at continental or global scales. Barbosa *et al.* (1997) used a multi-temporal multi-threshold approach to make continental burned area maps from 53 weeks of African AVHRR data. Burned pixels were labelled as those where the surface temperature increased and a vegetation index value decreased relative to statistical thresholds derived by examination of all 53 weeks of data. Eva and Lambin (1998) used a similar approach to label burned ATSR pixels in Central Africa using thresholds derived from other remotely sensed data. This letter describes a multi-temporal algorithm that uses a time series of burn scar index data to compute a burn scar index change map. The change map is then classified using thresholds derived from the output of an active-fire detection algorithm.

2. Approach

2.1. *Burn scar index*

A remotely sensed burn scar index that can discriminate between burned and unburned surfaces and is expected to be insensitive to smoke aerosols is used. Recent work using single date AVHRR data in Portugal has indicated that spectral vegetation indices that use the red (0.58–0.68 μm) and near-infrared (0.725–1.10 μm) channels give improved burned/unburned area discrimination when the red channel is replaced by the reflective component of the middle-infrared channel (3.55–3.93 μm) (Pereira 1999). In this study we use the VI3 index, originally proposed for studies of dense dark vegetation and aerosol reflectance, calculated as the near-infrared minus the reflective component of the middle-infrared divided by their sum (Kaufman and Remer 1994). Another burn scar index more suited to the MODIS spectral bands will be used for MODIS implementation of the algorithm

2.2. *Burn scar index change map*

A burn scar index change map is computed as the maximum minus the minimum burn scar index value found for each co-located pixel in the different orbits of data sensed over a given period. Figure 1 illustrates how a pixel which burns at some time during a ten day period will have a large burn scar index change value compared to the previous and subsequent periods when the pixel is unburned and burned respectively.

The period used to compute the change map is set at least equal to the satellite repeat cycle to ensure that variations caused by angular changes in the sensing and illumination geometry and surface reflectance anisotropy are captured (Meyer *et al.* 1995). The nominal satellite repeat cycle for AVHRR is approximately 9 days and for MODIS is 16 days which may cause a problem if the burned surface revegetates over these periods. Overlapping consecutive periods are used to ensure that fires that occur between periods are captured. An additional day of data is included at the end of each period that is also the first day of the following period (figure 1). Large changes may be produced by highly reflective (e.g. sunglint), cloudy, corrupted

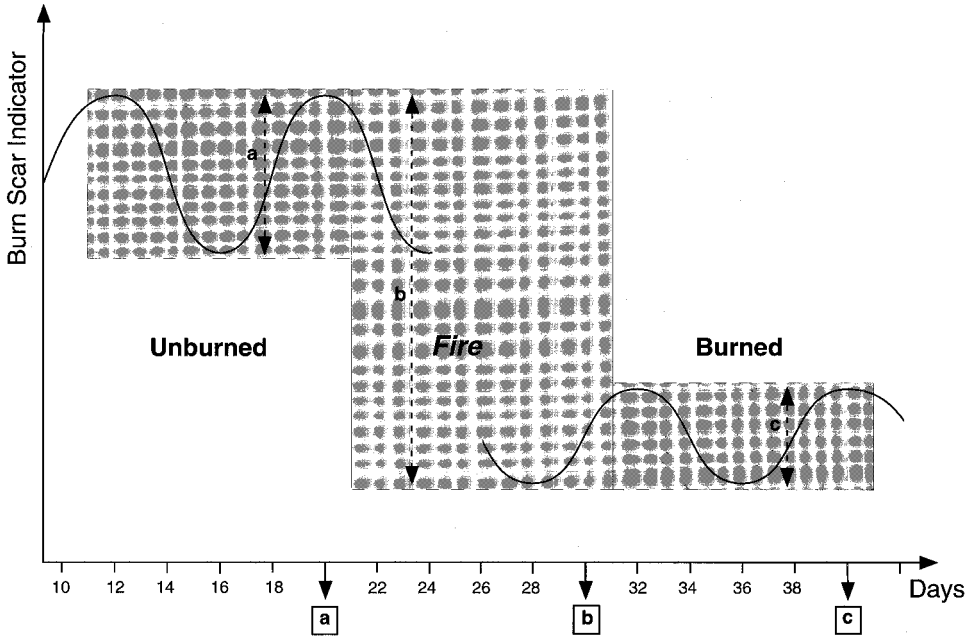

Figure 1. Burn scar index change map values computed for a single hypothetical pixel over three consecutive ten day periods. A fire occurs on day 25. The burn scar index change for the first unburned period (days 11–20) is *a*, for the second period (days 21–30) is *b*, and for the third burned period (days 31–40) is *c*. Note that the algorithm is applied to an additional unreported day of data at the end of each period.

and missing pixels. These are flagged and are not used. Saturated middle-infrared AVHRR pixels typically occur over surfaces with temperatures greater than 320° K and are flagged for use by the classification process.

2.3. *Burn scar classification*

The burn scar index change map is classified into burned and unburned pixels by thresholding. Thresholds based upon biophysical understanding of the behaviour of the burn scar index or derived empirically from another source of burned area information may be used. These approaches, however, are difficult to implement operationally and are sensitive to the data quality. For global applications the only adequate source of contemporaneous burned area information is that inferred from the application of an active fire detection algorithm.

An active-fire detection algorithm is applied to the different orbits of satellite data used to derive the burn scar index change map. The additional overlapping day at the end of each period is not considered. The locations of all change map pixels that were not saturated in the different orbits and where a fire was detected with high confidence are assumed to be burned. The values of the change map at these locations are used to define a statistical threshold to differentiate between burned (high burn scar index change values) and unburned (low burn scar index change values) pixels. For the results presented in this letter the mean and standard deviations of these values were used to derive thresholds for five classes (table 1).

Table 1. Burn scar classification thresholds.

Class	Lower threshold	Upper threshold
0 (unburned)	0	$\mu+1\sigma$
1	$\mu+1\sigma$	$\mu+2\sigma$
2	$\mu+2\sigma$	$\mu+3\sigma$
3	$\mu+3\sigma$	$\mu+4\sigma$
4(burned)	$\mu+4\sigma$	none

Class assigned to a pixel if the burn scar index change value is greater than or equal to the lower threshold and is less than the upper threshold. μ and σ correspond to the mean and standard deviation of burned scar index change values found at the locations of all pixels that were not saturated in the different orbits and where a fire was detected with high confidence.

3. Data

Twenty-four daily (afternoon pass) NOAA-11 AVHRR 1.1 km images sensed from 15 August to 15 September 1989 of an active burn near the Okavango Delta were examined. The data were processed using the Pathfinder II processing chain which incorporates an improved calibration method and corrects for Rayleigh scattering, ozone and water vapor absorption (El Saleous *et al.* forthcoming). Cloud screening was performed using the method of Saunders and Kriebel (1988). The reflective component of the middle-infrared channel was computed using the method of Roger and Vermote (1998). Pixels with middle-infrared channel brightness temperatures greater than 320° K were considered to be saturated. Active fires were detected by application of a recent algorithm that uses a contextual method and the near-infrared and thermal AVHRR channels (Giglio *et al.* forthcoming). The AVHRR images were corregistered manually with no more than one pixel root mean square error.

4. Results

Figures 2(*a*) and (*b*) show the normalised difference vegetation index (NDVI) and the burn scar index respectively for 6 September. This day was selected for illustrative purposes because it is cloud free and appears to show the spatial extent of most of the burning that occurred over the 24 days. The smoke plumes evident in the NDVI image are largely unseen in the burn scar index image which shows a considerably stronger discrimination between the burned and unburned areas. The Okavango Delta (north-west quadrant) appears bright in the burn scar index image because it is highly vegetated and moist, whereas the burned areas to the northeast and south of the delta are dark because of low post-burn moisture and vegetation levels. Figures 2(*c*) and (*d*) show the output of the burn scar detection algorithm applied to the first twelve days and to the last twelve days of data respectively. Five

Figure 2. An area of savanna burning near the Okavango Delta, Botswana, Southern Africa. The area illustrated corresponds to 360 by 360 NOAA-11 AVHRR 1.1 km pixels. (*a*) Normalised difference vegetation index image sensed on 6 September 1989. (*b*) Burn scar index image sensed on 6 September 1989. (*c*) Burn scar detection results for the first twelve days of the 24-day sequence. Shading corresponding to table 1 classes: black = unburned (class 0) and white = burned (class 4). (*d*) Burn scar detection results for the last twelve days of the 24-day sequence. Shading corresponding to table 1 classes: black = unburned (class 0) and white = burned (class 4).

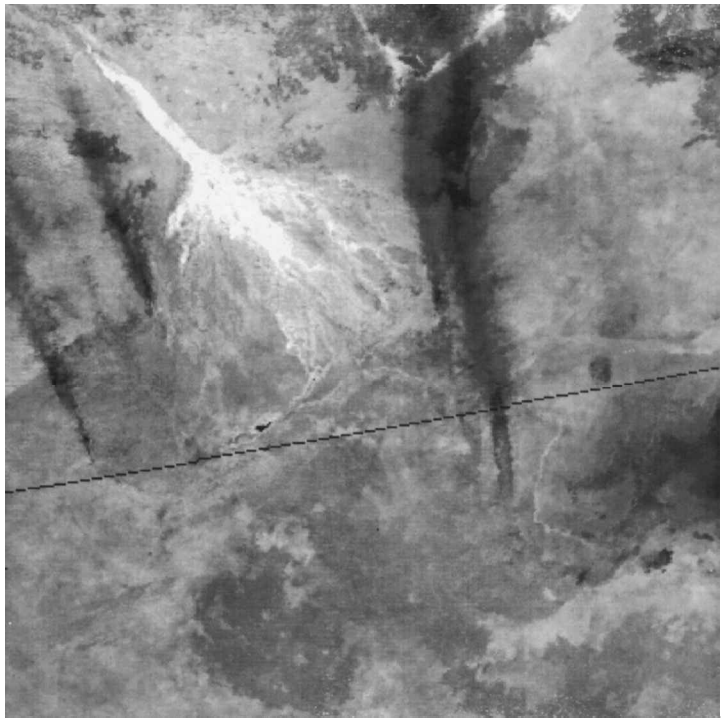

(*a*)

(*b*)

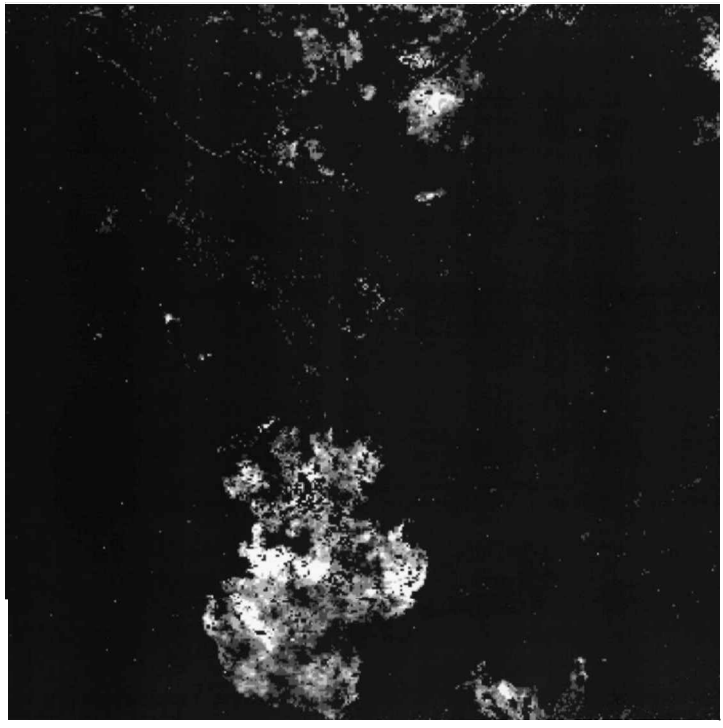

(*c*)

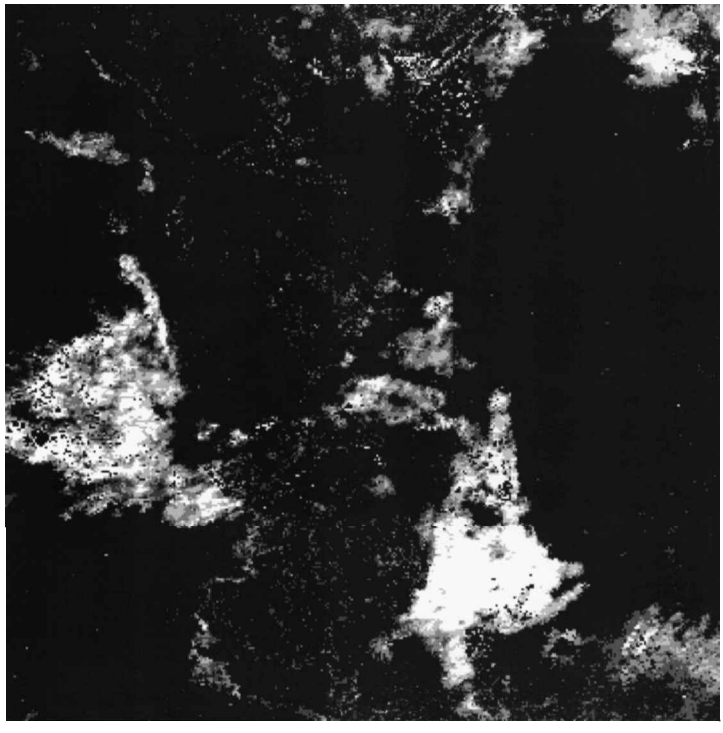

(*d*)

burn classes are shown which correspond approximately to the likelihood of burning (table 1). Generally, a strong spatial correspondence is observed between the burn scar detection results and the burned area seen in the NDVI and burn scar index images. It is suspected that some of the isolated pixels labeled as burned, including those along the edges of the Okavango Delta, are mislabelled because of AVHRR data processing problems which include data misregistration and inaccurate cloud detection.

5. Conclusion

A burn scar detection algorithm has been described that is based upon thresholding relative temporal changes in a burn scar index using the output of an active-fire detection algorithm. The area burned over a period at least equal to the satellite repeat cycle is mapped without iterative spatial or temporal searches and without using fixed thresholds except to detect saturated AVHRR pixels. The algorithm may be adapted to incorporate biophysically based thresholds and empirical thresholds derived from other sources of burned area information. Further work is required to investigate the spatial extent over which thresholds can be meaningfully applied because of sensitivity to the land cover and its properties and to the proportions of the pixels that are burned. Work is being performed to validate the algorithm quantitatively in different fire regimes around the world. The sensitivity of the algorithm to data misregistration and the subsequent impact upon burned area estimates is being investigated.

Acknowledgments

The authors acknowledge and thank Jose M. C. Pereira for his help and advice in the early stages of this work and Nazmi El Saleous for assistance with the Pathfinder II processing.

References

Barbosa, P. M., Gregoire, J.-M., and Pereira, J. M. C., 1997, Detection of burned areas in Africa using a multitemporal multithreshold analysis of NOAA-AVHRR-GAC data. In *Proceedings of SPIE, Earth Surface Remote Sensing*, edited by G. Cecchi, E. Engman, E. Ziloili (SPIE, Bellingham, Washington: SPIE), pp. 67–75.

Eva, H., and Lambin, E. F., Burnt area mapping in Central Africa using ATSR data. *International Journal of Remote Sensing*, **19,** 3473–3497.

Giglio, L., Kendall, J. D., and Justice, C. O., Evaluation of global fire detection algorithms using simulated AVHRR infrared data. *International Journal of Remote Sensing*, In Press.

IGBP, 1997, Definition and implementation of a global fire product derived from AVHRR data. International Geosphere-Biosphere Programme – Data and Information Systems (IGBP-DIS) Working Paper #17, Report of the 3rd IGBP-DIS Fire Working Group meeting, August 1997, IGBP-DIS office, CNRM, 42 avenue G. Coriolis, 31057 Toulouse, France.

Justice, C. O., Malingreau, J. P., and Setzer, A., 1993, Satellite remote sensing of fires: potential and limitation. In *Fire in the Environment; Its Ecological, Climatic and Atmospheric Chemical Importance*, edited by P. Clutzen and J. Goldmeyer (Chichester: John Wiley and Sons), pp. 77–88.

Kaufman, Y. J., and Remer, L., 1994, Detection of forests using mid-IR reflectance: An application for aerosol studies. *IEEE Transactions on Geoscience and Remote Sensing*, **32,** 672–683.

Meyer, D., Verstraete, M. M., and Pinty, B., 1995, The effect of surface anisotropy and viewing geometry on the estimation of NDVI from AVHRR. *Remote Sensing Reviews*, **12,** 3–27.

PEREIRA, J. M. C., 1998, A comparative evaluation of NOAA/AVHRR vegetation indices for burned surface detection and mapping. *IEEE Transactions on Geoscience and Remote Sensing*, **37,** 217–226.

PEREIRA, J. M. C., CHUVIECO, E., BEAUDOIN, A., and DESBOIS, N., 1997, A review of remote sensing methods for the study of large wildland fires, edited by E. Chuvieco, Report of the Megafires Project ENV-CT96-0256, August 1997, Universidad de Alcala, Alcala de Henares, Spain.

ROGER, J. C., and VERMOTE, E., 1998, Computation and use of the reflectivity at 3.75 μm from AVHRR thermal channels. *Remote Sensing of Environment*, **64,** 103–114.

SALEOUS, N. EL, VERMOTE, E., JUSTICE, C. O., TOWNSHEND, J. R. G., TUCKER, C. J., and GOWARD, S., AVHRR Land Pathfinder II: Improved algorithms for land studies. *International Journal of Remote Sensing*, **19,** 3473–3497.

SAUNDERS, R. W., and KRIEBEL, K. T., 1988, An improved method for detecting clear sky and cloudy radiances from AVHRR data. *International Journal of Remote Sensing*, **9,** 123–150.

SCHOLES, R. J., WARD, D., and JUSTICE, C. O., 1996, Emission of trace gases and aerosol particles due to vegetation burning in southern hemisphere Africa. *Journal of Geophysical Research*, **101,** 23677–23682.

WOLFE, R. E., ROY, D. P., and VERMOTE, E., 1998, The MODIS land data storage, gridding and compositing methodology: L2 Grid. *IEEE Transactions on Geoscience and Remote Sensing*, **36,** 1324–1338.